TPA−Silicalite Crystallization from Homogeneous Solution: Kinetics and Mechanism of Nucleation and Growth

Jonathan N. Watson,[†] Lennox E. Iton,[‡] Roland I. Keir,[§] John C. Thomas,[§] Trevor L. Dowling,[†] and John W. White*[,†]

Research School of Chemistry, Australian National University, Canberra, ACT, Australia 0200; Material Science Division, Argonne National Laboratory, Argonne, Illinois; and School of Physics and Electronic Systems Engineering, University of South Australia, SA, Australia

Received: May 7, 1997; In Final Form: September 8, 1997[⊗]

The formation and growth of tetrapropylammonium-templated crystal nuclei of silicalite from a clear homogeneous solution was recorded in situ as a function of time at temperatures between 90 and 115 °C using small-angle X-ray scattering (SAXS). The kinetics of the nucleation process was studied and give an apparent activation energy of 70 kJ mol^{-1}. A small-angle neutron scattering (SANS) contrast variation study confirms that the nuclei contain the tetrapropylammonium template in the expected stoichiometry of the completed crystal. Infrared spectroscopy provides evidence that the silicalite framework structure is present in the nuclei. Our SAXS and SANS data both show that a cylindrical form factor gave the best fit to the measured scattering functions for the particles that developed from nucleation to the end of the induction period. Dynamic light scattering measurements were used to follow the crystal growth in the 100−6000 Å size domain, beyond the range of the SAXS measurements. Scanning electron microscopy was also used to determine crystal morphology and particle sizes of sedimented crystals and freeze-dried solutions. We have proposed a detailed model for the nucleation and crystallization processes wherein cylindrical primary nuclei, 2 × 2 unit cells in cross section, form very quickly upon heating and then assemble end-to-end along the crystal *c* axis into 330 Å long primary crystallites during an extended induction period, followed by the aggregation of the primary crystallites into polycrystalline ellipsoids of length 6000 Å.

Introduction

In their 1985 review,[1] Lok et al. identified zeolite crystallization as one of the most complex chemical problems of the time. We have previously used scattering methods[2,3] to identify the first steps in the template-induced structuring process of gels, but the complexity of scattering is greatly reduced by using clear synthesis solutions. Our recent report[4] on these systems for silicalite synthesis defines the method and shows its efficacy. Here we follow the process through to crystallization and give the detailed evidence for template inclusion and the thermodynamics. The scattering is simple enough that a semiquantitative interpretation of it can be given in terms of the classical mechanisms[5,6] of template action. Previously, we have shown[2] by small-angle neutron scattering (SANS) that in a gel-based silicalite synthesis mixture a very high degree of template incorporation into the gel occurred at room temperature soon after the mixing of components.

There has been recently much interest in the small-angle X-ray and neutron scattering[7−9] and in the light scattering[10−14] from preparations of ZSM-5 and silicalite, using tetrapropylammonium (TPA) cations as the organic structure-directing agent. The TPA ions are located at the channel intersections with the propyl chains extending into both the linear and sinusoidal channels and, consequently, must be incorporated into the framework during crystal growth as they are too large to enter the channels after crystallization.[6] The crystalline unit cell of the templated silicalite[15] is orthorhombic (***Pnma***) and has dimensions $a = 20.06$, $b = 19.80$, and $c = 13.36$ Å.

Regev et al.[7] studied the small-angle X-ray scattering (SAXS) from the mother liquor above a gel-based preparation of ZSM-5 with a silicon to TPA ratio of less than 2. (The silicon to TPA ratio in the final product is 24:1.) The unheated mother liquor from this gel contained 50 Å spherical particles, and these particles were present throughout the hydrothermal reaction. The surmise of Regev et al. was that these "globular structural units" were comprised of several "tetrapods" though they did not confirm directly the inclusion of TPA in the particles. Regev et al. also found that neither the shape nor the size of the particles in the mother liquor changed after the first 2 h of heating thereby defining their nucleation period. During the nucleation period, aggregation of the 50 Å globular structural units occurred with the formation of cylindrical particles of dimensions 160 × 440 Å. These aggregates seemed to settle into a disordered precipitate but subsequently ordered into ZSM-5 with further heating.

Experiments more closely related to those reported here were performed by Twomey et al.,[10] who followed the crystallization of silicalite from a clear solution using light scattering methods. The study of zeolite crystallization kinetics is simplified by employing clear solutions since a coexisting solid amorphous phase is not present. A particularly interesting finding of Twomey et al. was that aging at room temperature increased the number density of the growing nuclei and the crystal growth rate. Heating was required to enable the formation of nuclei that could sustain further growth. The DLS experiments in their study were unable to observe the formation of inactive germ nuclei (sizes <200 Å).

Ex situ light scattering experiments were conducted by Schoeman et al.[11] on the clear solutions in their preparation of colloidal silicalite. Again, the dynamic light scattering measurements made in these studies were unable to resolve particles

* To whom correspondence should be addressed.
[†] Australian National University.
[‡] Argonne National Laboratory.
[§] University of South Australia.
[⊗] Abstract published in *Advance ACS Abstracts,* November 1, 1997.

S1089-5647(97)01531-9 CCC: $14.00

with sizes below 200 Å so their failure to see smaller particles in the unheated solutions is not definitive. These studies all conclude, however, that the crystallization occurs with a constant number of spherical particles whose diameters increase linearly with time. This is not the same scenario at present in the experiments of Regev et al.

Schoeman[14] most recently reported an in situ laser light-scatterng study of the initial stage of crystallization of TPA−silicalite. In these experiments, colloidal particles (33 Å) were detected throughout the crystallization. After heating at 70 °C for 9.5 h he found that a second discrete particle population (120 Å) had formed in the solution. By deconvoluting the intensity data during this period, the larger particles were shown to have originated from subcolloidal particles initially present in the solution before heating. The results also indicate that the initial crystal growth rate of the crystals is a nonlinear function of time until an average particle size of 200 Å is attained, after which it becomes linear. As will be seen, our results agree satisfactorily with Schoeman with the important difference that there was no detectable X-ray scattering from the clear start solution before heating.

Another recent SAXS study is that of Dokter et al.[8] which looks at homogeneous versus heterogeneous zeolite nucleation. They used the concept of fractal dimension to interpret SAXS patterns and proposed a mechanism of microstructural random packing, subsequent ordering, and crystallization for the homogeneous system. The main steps involved in this process are as follows: (1) formation of silicate−TPA clusters in solution, (2) primary fractal aggregates formed from the silicate−TPA clusters, (3) densification of these primary fractal aggregates, (4) combination of the densified aggregates into a secondary fractal structure and crystallization, and (5) densification of the secondary aggregates and crystal growth. However, in this study, and in all of the above studies as well, there is no direct evidence of the template incorporation in these particles although it might be presumed since the final product is silicalite.

The work reported here is concerned with following the template-induced crystallization from its earliest stages to recognizable crystals in the electron micrographs of materials from the synthesis solutions. A tetrapropylammonium ion templated synthesis of silicalite from a totally clear, nongelling solution was followed in situ by small-angle X-ray scattering during the nucleation period as a function of time for temperatures between 90 and 115 °C. SAXS experiments give the size, number, and dimensionality of the scattering species. From these results we were able to determine the rate of growth of silicalite nuclei (as a function of radius of gyration) during the nucleation process as well as the apparent activation energy for nucleation. SANS as a function of D_2O/H_2O contrast is then used to show that the nuclei are indeed templated. Further evidence of the silicalite structure in the early stages of particle growth is provided by infrared spectroscopy. Dynamic light scattering (DLS) was used to measure the crystal growth rate of silicalite at 100 °C for sizes above 200 Å. Scanning electron microscopy (SEM) was used to analyze samples taken at several different stages during the synthesis, thereby enabling changes in crystal morphology to be monitored during their growth.

Experimental Section

Synthesis Solutions. The synthesis mixture on which the detailed crystallization studies were conducted was a "water white" solution with a silicon to TPA ratio of 8.3:1. This ratio means that the system is not strongly forcing, but X-ray diffraction shows that it crystallizes silicalite at 100 °C after heating for 36 h. The silicalite synthesis solution was prepared by stirring a TPA−Br (Aldrich) solution into a sodium silicate solution (E-Brand, PQ Corp.) to give a clear homogeneous solution with the following molar composition

$$1.0\ SiO_2{:}0.297\ Na_2O{:}0.12\ TPA{-}Br{:}120.0H_2O$$

The above solution differs from the clear solutions devised by von Ballmoos[16] (and used by us previously[3]), particularly in the ratio of silica to TPA (8.3:1 versus 1:2). To get nongelling solutions, the gelling properties of a broad suite of starting mixtures were studied. The compositions of the solutions examined are summarized in Table 1. The molal concentrations of TPA−Br in the solutions range between 0.042 and 0.578, and the effective molal concentrations of SiO_2 in the solutions range between 0.463 and 2.891. We refer below to relative concentrations within these ranges as high or low but point out that the studies reported by others[7−11] on silicalite crystallization from homogeneous solutions are based mainly on solutions that are much more concentrated than the solution composition that we use in this study.

TABLE 1: Molar Compositions of TPA−Silicalite Syntheses Solutions

	moles			
solution	SiO_2	Na_2O	TPA−Br	H_2O
type A	1.0	0.297	0.03	40.0
(hetero)	33.3	9.9	1.0	1333.3
type B	1.0	0.297	0.12	120.0
(homo)	8.33	2.47	1.0	1000.0
type C	1.0	0.297	0.06	80.0
(hetero)	16.67	4.95	1.0	1333.3
type D	1.0	0.297	0.09	96.0
(homo)	11.1	3.3	1.0	1066.7
type E	1.0	0.297	0.2	19.2
(gelled)	5.0	1.485	1.0	96.1
type F	1.0	0.297	0.1	55.6
(hetero)	10.0	2.97	1.0	555.6
type G	1.0	0.297	0.1	55.6
(hetero)	5.0	1.485	1.0	277.8

Crystallization Behavior. In that which follows we will use the term *heterogeneous crystallization* to describe those crystallizations in which a visible gelatinous intermediate always occurred; conversely, we will use the term *homogeneous crystallization* to describe those crystallizations in which no visible gelatinous intermediate ever occurred. The term gelation is used to describe the formation of a dense gel after mixing the sodium silicate and TPA−Br solutions. As we will show, the model we have developed in this paper for the crystallization process in the homogeneous case does not depend on nucleation at the interface of an amorphous mass.

For solution A, the SiO_2 concentration is high and the SiO_2:TPA−Br ratio is high. Silicate polymerization is fast, and a small amount of suspended gel is formed quickly (in the first day) at 100 °C. Despite the fact that the starting solution is clear heterogeneous crystallization of TPA−silicalite prevails, and the crystalline product can be recovered in 3 days.

For solution B, the SiO_2 concentration is low and the SiO_2:TPA−Br ratio is low. Silicate polymerization is slow, and no suspended gel is formed at 100 °C. Instead, homogeneous crystallization of TPA−silicalite prevails (presumably because of the high TPA:SiO_2 ratio), and the crystalline product can be recovered in (2 to) 3 days.

For solution C, both the SiO_2 concentration and the SiO_2:TPA−Br ratio are at intermediate values. Silicate polymerization is slow at 100 °C, but homogeneous nucleation is even slower. A suspended gel is formed very slowly; a very small quantity is evident after 3 days, and a significant quantity of

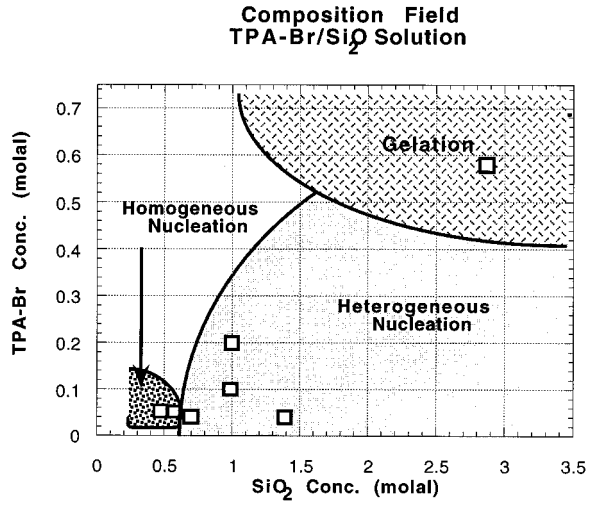

Figure 1. Crystallization field for TPA−silicalite.

more compact gel is suspended after 9 days. As in the case of solution A, heterogeneous crystallization of TPA−silicalite occurs, and the crystalline product can be recovered after 17 days.

For solution D, both the SiO_2 concentration and the SiO_2:TPA−Br ratio are at low intermediate values. Silicate polymerization is slow at 100 °C, and no gel is formed. Homogeneous crystallization occurs, though less quickly than for the type B solution. A colloidal suspension is present after 40 h, and sedimentation of the product appears to be complete after 7 days.

Solution E was formulated so that the H_2O:SiO_2 and SiO_2:TPA ratios were equivalent to one (S3) used in the suite studied by Persson et al.[12] The concentrations of both SiO_2 and TPA are the highest used in our suite of mixtures. A dense gel formed promptly upon mixing the components because the TPA in our formulations is in the form of the bromide rather than the hydroxide and because Persson et al. also included a substantial amount of ethanol as a cosolvent in their preparation.

Solutions F and G were close to solutions S11 and S10 of Persson et al.[12] in their respective H_2O:SiO_2 and SiO_2:TPA ratios. Solutions F and G have the same SiO_2 molality, but solution G has the same SiO_2:TPA ratio as the concentrated solution E. Both solutions F and G formed gelatinous intermediates in suspension and underwent heterogeneous crystallization that was complete in about 7 days.

From these data it is possible to give the outlines of a diagram indicating the crystallization behavior of the systems. This is shown in Figure 1. We have chosen the synthesis solution of composition B for the detailed study of the crystallization that we present in this paper. The effective molality of SiO_2 in this solution is 0.463, and the molality of the TPA−Br is 0.056. At this concentration in an aqueous solution containing no silicate, TPA-Br is almost completely ionized, with a small concentration of ion pairs and a negligible concentration of ion pair dimers.[17]

Small-Angle X-ray Scattering. Small-angle X-ray scattering measurements were performed in the Research School of Chemistry at the Australian National University using the SAXS camera which is described elsewhere.[18] With the development of a very efficient and precisely controllable high-temperature stage on our small-angle camera, we were able to perform in situ measurements of the scattering function as the reaction proceeds. Since good scattering functions were able to be recorded for exposure times of 20 min, the early and later stage time developments of the scattering function could be studied with reasonable precision so as to obtain kinetic and thermodynamic parameters of the nucleation reaction.

The intensity of small-angle scattering, *I(Q)*, whether it be X-ray or neutron scattering, is given by the general equation

$$I(Q) = \phi P(Q)\, S(Q) \tag{1}$$

where ϕ is the number density of particles in solution and Q is momentum transfer ($\sin \theta 4\pi/\lambda$, where θ is the half scattering angle and λ the X-ray wavelength). The form factor, *P(Q)*, reflects the distribution of scattering material in the scattering particle, and the structure factor, *S(Q)*, is related to the spatial distribution of the scattering particles in the solvent. For dilute solutions *S(Q)* is a constant and where also precision is limited by counting statistics, the scattered intensity may be represented by that from spherical particles as a first approximation using the Guinier relation

$$I(Q) = I(0) \exp(-Q^2 R_g^2/3) \tag{2}$$

For the 2 h runs where there were good counting statistics, it was reasonable to fit a form factor to the whole scattering function. It became apparent that a cylindrical form factor was a good approximation to the data for the nuclei. To calculate the cross-sectional radius of gyration R_c (defined as the second moment of the distribution of the scattering density) from the scattering curve, plots of $\ln(QI)$ vs Q^2 were constructed from which R_c was obtained from the slope using eq 3:

$$\ln QI(Q) = \text{const} - {}^1/_2(Q^2 R_c^2) \tag{3}$$

The whole data field was also used to construct the radial distribution function *P(r)* for some typical cases. This function is used to illustrate the size distribution of nuclei in the first stages of growth. *P(r)* is the probability of an interatomic distance *r* inside the particle such that the point at which the function goes to zero represents the maximum distance between atoms in the particle. Strong artificial oscillations in the *P(r)* function occur due to the termination effect (due to the instrument setup prohibiting the measurement of the scattering curve down to zero angle) and the influence of a remaining background. To remove the oscillations, it was necessary to extrapolate the experimental data to zero angle and trim the data at larger angles. The extrapolation of the scattering curve was achieved by fitting a fourth-order polynomial to the experimental data. To check the validity of this extrapolation, a cylindrical form factor was fitted to the extended scattering curve, and no significant change in the dimensions of the cylinder was found when compared to the original experimental data.

To analyze the kinetics and to give an overview of the nucleation and growth in the system, Guinier plots were constructed by plotting the log of the intensity, *I*, versus the square of the momentum transfer, *Q*, for each run from which the radius of gyration, R_g, and scattering intensities *I(0)*, were determined (eq 1).

Small-Angle Neutron Scattering. *Contrast Variation Study.* The intensity *I(Q)* of the small-angle scattering from a solid particle depends on the difference in scattering length density ($\rho_m - \rho_s$) between the solid, ρ_m, and solvent, ρ_s, phases, as shown in eq 4.[19] Isotopic substitution can be exploited in SANS

$$I(Q) = k(\rho_m - \rho_s)^2 S(Q) \tag{4}$$

to substantially change the contrast between the solvent and solid components. By independently labeling the templated solid and solvent isotopically with hydrogen or deuterium, the

TABLE 2: Calculated Scattering Length Densities for Silicalite

material	scattering length density (10^{10} cm^2)	scattering length density equivalent (wt % D_2O in D_2O/H_2O)
d_{28}-TPA−Si−ZSM-5	4.87	80.4
h_{28}-TPA−Si−ZSM-5	2.66	49.3
Si−ZSM-5	2.78	51.0
colloidal silica	3.48	61.1
H_2O	−0.562	0
D_2O	6.34	100

scattering intensity as a function of solvent scattering length density can be measured. When the scattering length density of the fluid and solid components are matched ($\rho_m = \rho_s$), the scattering intensity will be nulled ($I(0) = 0$). Hence, the scattering length density of the particles can be determined. The scattering length densities for crystalline silicalite containing *h*-TPA, *d*-TPA, and dense amorphous silica are given in Table 2. In this study, we use the methods developed before[2,3] and vary the scattering length density of the solvent by changing the D_2O/H_2O ratio in the solution. Also, by using both hydrogenated (h_{28}-TPA) and deuterated (d_{28}-TPA) template, the scattering length density of the nuclei was varied. For a selected heating time of the synthesis solutions, a contrast variation series of SANS measurements for each template was made. The SANS patterns were measured on the small-angle diffractometer SAD at IPNS, Argonne National Laboratory.

Ex Situ SANS Study. In addition to the above contrast variation study, an ex situ SANS study of the crystallization of silicalite at 100 °C was also performed using the LOQ small-angle scattering instrument at the Rutherford Appleton Laboratory, UK. The results from this study were used to complement the in situ SAXS measurements.

Dynamic Light Scattering. The dynamic light scattering measurements were preformed in the School of Physics and Electronic Systems Engineering at the University of South Australia using a BI-200SM stepper-motor controlled goniometer system (Brookhaven Instruments) fixed at 90°. The light scattering apparatus was as previously described[20] with the exception of the laser which was an argon ion laser (Lexel, Model 95) operated at either 150 or 350 mW (depending on the particle size) and a wavelength of 488 nm. The temperature at the time of the recording of the measurements was 25 °C. To calculate particle diameters from DLS measurements, it is necessary to assume that the particles are spherical and that the radius of the particle is related to its diffusion coefficient. (Particle diameters were determined by second-order cumulants (and fourth-order cumulants in the case of particles smaller than 200 Å) analysis.) This approach differs from small-angle X-ray and neutron scattering where the form factor of the (small) particles can be measured to provide shape information.

Other Experiments. Infrared spectroscopy was performed on a Perkin-Elmer 1800 FTIR instrument. Freeze-dried samples were collected during the early stages of the synthesis when the solution still appeared clear, otherwise, the filtered product was collected. All of the IR samples were prepared as KBr pellets.

Field emission scanning electron microscopy was performed using a Hitachi 4500 microscope. Samples for analysis were collected by filtering the synthesis solution or by freeze-drying the synthesis solution which was heated for a given time. Silver paint was used as an adhesive for securing the specimen to the stub before being gold coated.

TABLE 3: In Situ SAXS Study of the Rate of Increase in R_g (Å) and $I(0)$ during the Synthesis of Silicalite

	temp/°C					
time/min	90	95	100	105	110	115
			R_g (Å)			
20	37	38	43	44	47	61
40	40	42	46	49	54	79
60	43	47	52	58	60	89
80	44	48	52	63	69	92
100	45	49	60	69	84	89
120	45	51	64	77	86	84
140	49	57	67	77	79	
160	51	58	69	77	82	90
180	54	63	64	77	81	
200	56	65	-	83	87	90
220	58	63	71	84		
240		64	78	83	85	
			I (0)			
20	11	12	21	37	34	71
40	20	19	28	55	52	121
60	26	24	36	73	69	150
80	28	27	39	85	80	160
100	31	30	46	101	103	160
120	32	32	52	112	112	151
140	36	35	55	120	103	
160	39	37	61	125	109	165
180	43	40	59	130	110	
200	45	43		145	123	162
220	48	45	66	144		
240		64	76	145	118	

Results and Discussion

Growth of Silicalite Particles. *SAXS Data*. For each of the SAXS experiments an aliquot of a freshly mixed solution was sealed in a 1.0 mm capillary and placed in the heater of the small-angle scattering machine which was set at the following temperatures: 90, 95, 100, 105, 110, and 115 °C. An uncertainty of ±0.2 °C was recorded for each of the set temperatures. The scattering function was first measured over 20 min periods for 6 h at each temperature. In a second experiment, in situ measurements were then performed which involved taking 2 h time shots for 32 h at 100 and 110 °C. A fresh unheated silicalite synthesis mixture (1.0 mm capillary) was used in the analysis for background correction. (Previously we used a water background in the analysis.[4]) Flux and transmission measurements were taken before and after the runs to provide absolute intensities. The corresponding Guinier analysis for each run is summarized in Tables 3 and 4.

Preliminary Analysis. The SAXS pattern for the unheated silicalite solution after preparation showed little scattering above a water background. The radius of gyration, R_g, was certainly less than 10 Å. After heating for 20 min at 100 °C, particles with a radius of gyration of the order of 43 Å were observed. With continued heating Guinier fits to the scattering function were not inconsistent with the presence of two particle "populations". One, which scattered weakly, could be parametrized with $R_g = 43$ Å and another showing an increasing radius of gyration and scattering intensity with time. For this second "population" the maximum size and scattering intensity were reached at the 14 h mark. For the kinetic experiments attention was focused on this part of the scattering curve. After 14 h, there is a continual decrease in the scattering intensity over the next 18 h with no larger particles being detected by SAXS. The presence of the $R_g = 43$ Å particle throughout the crystallization is consistent with the observations reported by Schoeman,[14] but detailed fits of the form factor (below) illustrate that the matter needs more attention since a single cylindrical form factor is a

TABLE 4: In Situ SAXS Study of the Crystallization of Silicalite at 100 and 110 °C

	100 °C		110 °C	
time/h	R_g/Å	$I(0)$	R_g/Å	$I(0)$
0−2	63	79	54	63
2−4	74	141	75	168
4−6	78	176	84	213
6−8	83	207	80	206
8−10	81	205	80	209
10−12	92	244	77	200
12−14	90	238	75	177
14−16	92	242	74	154
16−18	94	237	74	136
18−20	94	216	68	113
20−22	93	201	70	101
22−24	97	207	68	85
24−26	93	181	75	80
26−28	102	212	73	70
28−30	97	185	83	64
30−32	92	124	76	34
32−34	105	97	77	12

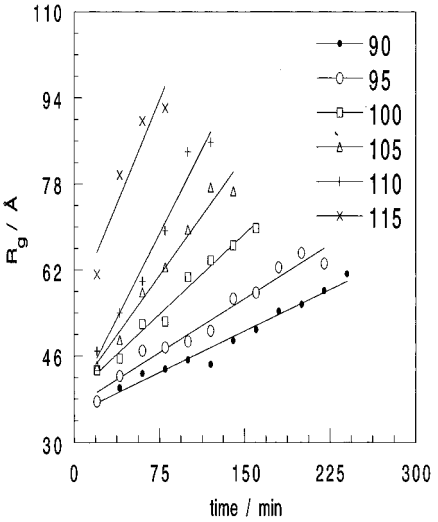

Figure 2. Change in the radius of gyration (measured by the spherical Guinier approximation) at different times and temperatures.

good fit to all of the data in the Q range studied. Ex situ SAXS measurements were performed at 100 °C, and they showed excellent agreement with the in situ results.

Observations on a bulk silicalite preparation heated in an oven at 100 °C showed that the solution remained clear until after approximately 14 h of heating when it became faintly cloudy. This point in time corresponded to that when $I(0)$ reached a maximum (see Table 4). Continued heating of the solution resulted in a more concentrated sol with sediment being first observed after 24 h. A decrease in $I(0)$ was recorded over this period of time. Heating for 32 h produced particles that were already substantially sedimented.

The effect of increasing the synthesis temperature is shown in Table 4, where the length of the induction time (defined here as the time taken for the value of $I(0)$ to reach a maximum) decreased from 12 h at 100 °C to 6 h at 110 °C. Table 3 displays a similar trend at all six temperatures for the shorter 20 min runs, whereby the nuclei grow in size during the induction period, together with an increase in $I(0)$.

Using the data in Table 3 to calculate particle growth rates based on the increase in the radius of gyration, R_g (Figure 2), gives an estimation of the apparent activation energy for the growth in the particle radius, assuming that the rate is described by the Arrhenius equation. A good straight line Arrhenius plot (Figure 3) was obtained which gave 70 kJ mol^{-1} for the apparent

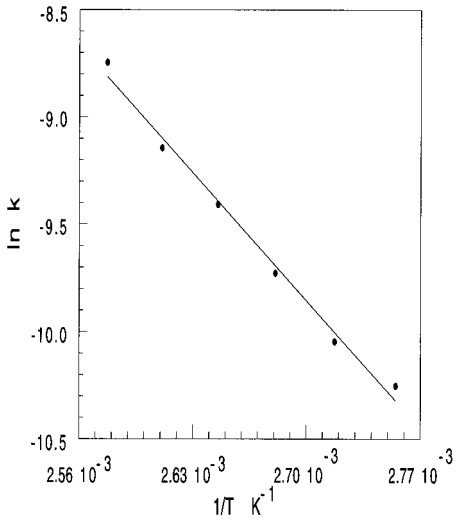

Figure 3. Arrhenius plot used to calculate the apparent activation energy for growth in radius of silicate nucleii.

TABLE 5: Ex Situ SANS Study of the Crystallization of Silicalite at 100 °C

t/h	$I(0)$	R_g/Å	t/h	$I(0)$	R_g/Å
0	0.0483	19	19	1.064	93
1	0.063	39	22	0.7619	88
3	0.2923	57	26	0.844	91
5	0.3957	66	30	1.114	106
11	0.4177	78	36	1.033	148
14	0.6288	87	48	0.760	160
16	1.075	100			

activation energy of growth. This result is comparable with other reported values[10,11] and suggests a surface reaction-controlled growth mechanism rather than a diffusion mechanism (E_a = 12−17 kJ mol^{-1}).[21]

SANS Data. A silicalite solution made up with 94.5 wt % D_2O was divided into 20 separate samples. This D_2O concentration was chosen to provide a good contrast between the scattering species and the solvent and, also, to minimize the amount of incoherent scattering due to the presence of hydrogen. Each sample was sealed in a polyethylene bottle and placed in an oven set at 100 °C for a given time ranging from 1 to 46 h. Samples were quenched in cold water after they were removed from the oven and then transferred to quartz cells 1.0 mm thick. In this series of measurements, such as the SAXS measurements, the unheated synthesis mixture was used as the background. Results from the Guinier analyses for all of the samples are shown in Table 5. The R_g values and the trend in $I(0)$ compare very well with the SAXS results given in Table 4. Observations were recorded over the same Q range for both the SAXS and SANS measurements.

DLS Data. Aliquots (2 mL) of the silicalite starting solution were transferred to small borosilicate tubes (12 × 75 mm) which were then sealed. The tubes were placed in an oven at 100 °C and left for a given synthesis time, after which the tube was quenched in water and the particle size was measured. At each time interval the particle size was determined three times using a measurement time of 5 min. At synthesis times above 20 h it was necessary to open the tubes and dilute the sample by 2 orders of magnitude to reduce the possible occurrence of multiple light scattering. The dynamic light scattering measurements given in Table 6 indicate that the nucleation period for the synthesis at 100 °C was approximately 12 h, after which there was a rapid increase in the average particle size until the reaction slowed at around 35 h.

TABLE 6: Ex Situ DLS Study of the Crystallization of Silicalite at 100 °C

time/h	*d*/nm	time/h	*d*/nm
1	11	17	120
2	16	18	132
3	14	19	161
4	15	20	191
5	16	21	198
6	17	22	250
7	17	23	256
10	29	24	335
11	31	26	355
12	35	35	547
13	42	40	568
14	53	45	589
15	89	50	600
16	89		

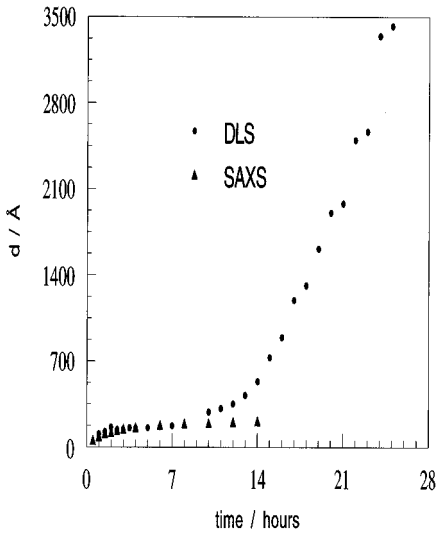

Figure 4. Combined SAXS and DLS measurements monitoring the growth of silicalite nuclei and crystals at 100 °C.

Although it was necessary to assume that the silicalite particles were spherical for the analysis of the DLS data, this may not be totally correct (especially during the early stages of crystallization as will be discussed in a later section), and therefore some uncertainty must be associated with the "hydrodynamic" particle diameters. The most important observation to note from the DLS data is, however, the clear agreement with the SAXS data (above ca. 200 Å) about the particle size at the onset of crystallization. The length of the nucleation period is in excellent agreement with the SAXS results. The initial growth period of the particles was difficult to determine using DLS because at this point the particles were small (<200 Å) and few in number, leading to poor signal to background.

A second study was done in the nucleation period below 7 h, and the results are also included in Table 6. To reduce the presence of dust/background and to increase the signal from the particles, the solution was filtered through a 0.22 mm filter, the laser power was increased to 350 mW, and the measurement time was doubled. For this study it was necessary to use data obtained from the fourth-order cumulants analysis because the particle size distribution in this region was polydisperse. Furthermore, the particles were small and few in number during the nucleation period, and this significantly affected the convergence of the cumulants analysis. A comparison of the DLS and SAXS data below 24 h is given in Figure 4 where the complementary nature of the experiment is evident. The SAXS radii were converted to physical diameters obtained from DLS. Here, the SAXS easily determines the presence of particle sizes up to 100−150 Å but loses them above this range whereas DLS

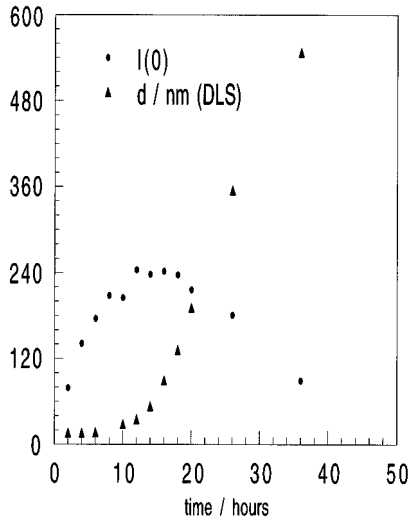

Figure 5. Plot showing the trend between the decrease in $I(0)$ measured by SAXS with the onset of crystal growth monitored by DLS.

resolves the larger particle diameters (>200 Å) quite easily. It is evident from the figure that if great care is taken in sample preparation for DLS, it is possible to measure particle growth during the initial nucleation period with some degree of accuracy, although SAXS is a much better method. Figure 5 compares the increase in the crystal size measured by DLS with the $I(0)$ values obtained from SAXS. The graph clearly shows that once crystallization begins there is a corresponding decrease in the $I(0)$ values for times in excess of ≈12 h.

Characterization of the Silicalite Particles. *SANS Contrast Variation Data*. Two sets of five solutions of the synthesis mixture were prepared with different solvent scattering length densities of 94, 72, 53, 32, 21 wt % and 94, 83, 72, 53, 32 wt % D_2O in D_2O/H_2O for h_{28}-TPA and d_{28}-TPA, respectively. These solutions were then heated in an oven at 100 °C for 5 h. This particular heating time was chosen so that the scattering produced by the samples was strong enough to enable reliable data to be gathered with sampling times of 4−5 h, yet still provide evidence for the incorporation of the template at the earliest possible stage of the observed particle growth shown by SAXS. Background solutions corresponding to the above concentrations of D_2O in D_2O/H_2O were measured to correct for incoherent background scattering due to the presence of hydrogen atoms in the solution. Samples were contained in quartz cells, 1 or 2 mm thick depending on weight percent of D_2O, and sealed with paraffin.

Scattered intensity profiles for some of the heated solutions are shown in Figure 6. A significant point that is illustrated by these spectra is that contrast nulling occurs over the whole Q range of the instrument at 53% D_2O and 73% D_2O for *h*-TPA and *d*-TPA, respectively, thereby indicating that the scattering particles are homogeneous.

Our small-angle neutron scattering study[4] using hydrogen and deuterium contrast variation has shown that the TPA template is incorporated into the R_g = 94 Å particles. The contrast variation plots for h_{28}-TPA and d_{28}-TPA are shown in Figure 7. $I(0)$ values were obtained from Guinier plots. It is obvious from the two plots that the scattering from the silicalite solution is sensitive to the isotopic labeling of the TPA template. For h_{28}-TPA and d_{28}-TPA template the contrast null point occurs at 60 and 75 wt % D_2O/H_2O, respectively. These results compare very well with the predicted and experimental values for scattering length density equivalents of weight percent D_2O/H_2O for zeolite materials given in Table 2. This proves that

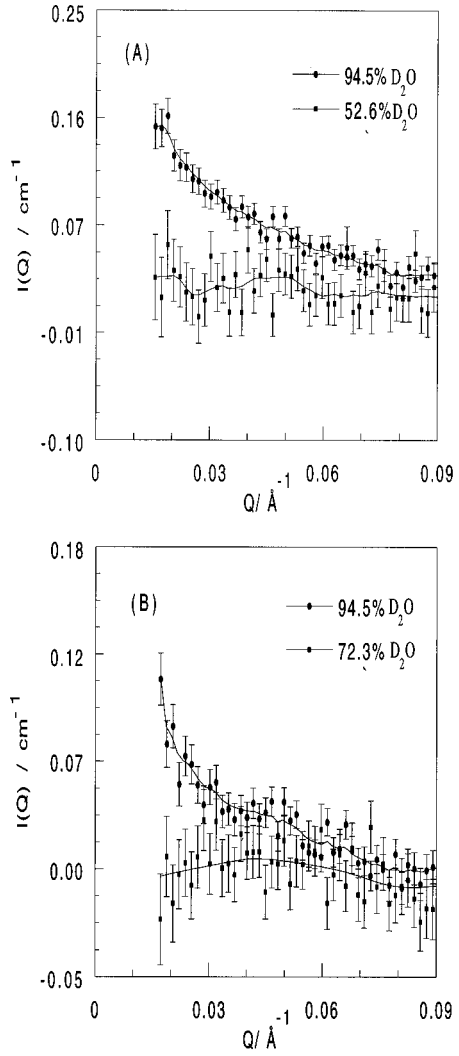

Figure 6. SANS scattering patterns for (A) *h*-TPA and (B) *d*-TPA silicalite nuclei at different H_2O/D_2O contrasts.

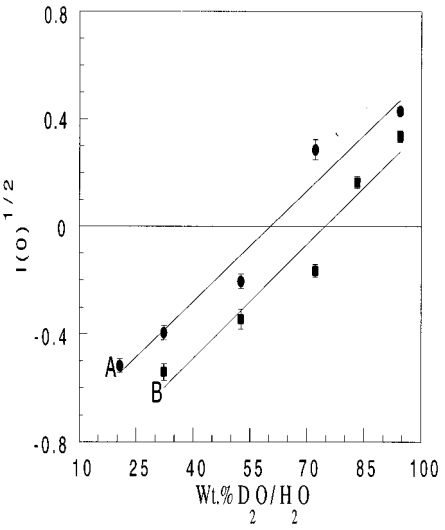

Figure 7. Contrast variation plots of SANS intensities for silicalite solutions heated for 5 h at 100 °C with (A) *h*-TPA and (B) *d*-TPA template.

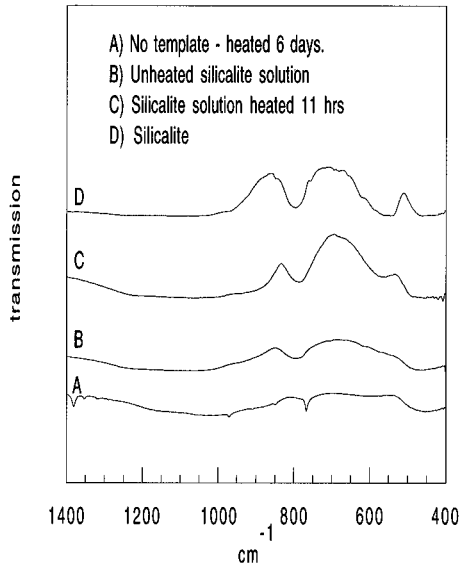

Figure 8. IR spectra of samples taken from a silicalite synthesis solution after different heating times.

the 94 Å particles have a density which is nearly that of a fully densified silicalite particle containing the TPA template.

Further supporting evidence relating to the structure of the 94 Å particles is obtained using infrared spectroscopy. The IR spectrum of silicalite is characterized by two structural vibrational bands in the spectra region of 400−700 cm^{-1}. The band at 440−470 cm^{-1} is a Si−O bending mode observed in many polymorphs of SiO_2. However, the appearance of a second band at 550−560 cm^{-1} is indicative of the MFI structure (silicalite) and is not observed in amorphous silica.[22] As shown in Figure 8, a band at 560 cm^{-1} is present in the spectra of the crystallized sample and for a sample that was taken from the synthesis mixture after being heated for 11 h at 100 °C. This band is notably absent from the spectrum for the sample taken from the freshly prepared unheated synthesis solution. The XRD pattern obtained from the sample that was heated for 11 h was shown to be amorphous by standard X-ray techniques despite showing the spectroscopic signature of the MFI framework of silicalite. This suggests that the relatively small silicalite particles only contain order over length scales of a few unit cells.[23] During the induction period in our system there are no detectable particles in the synthesis solution larger than the 94 Å particles measured by SAXS and DLS, and hence, it must be the structure of these particles that give rise to the band at 560 cm^{-1}. Therefore, from the combination of the SANS results (which found the 94 Å particles to have a scattering length density almost equivalent to that of TPA templated silicalite) and the IR result (showing the appearance of the band at 560 cm^{-1}), it can be confidently stated that the 94 Å particles are silicalite nuclei and that we are observing the nucleation process.

Shape of the Silicalite Particles. *SAXS and SANS.* The parameters obtained from fitting a cylindrical form factor to the SAXS and SANS data at different heating times are summarized in Table 7. These parameters were used to calculate values of R_g included in Table 7 from the cylinder radius, R, and its length, L, by a standard geometric expression. Figure 9 illustrates several examples of the form fitting to the data where the agreement shown between the calculated and experimental curves in all of the graphs is excellent. Also given in Table 7 are values of R_c obtained from $\ln(QI)$ vs Q^2 plots (Figure 10) using the SAXS and SANS data. The two experiments show the same trend in growth with heating time where a small increase in the radius of the cylinder is recorded together with a large increase in the length of the cylinder until reaching a maximum detectable size of $R = 44$ Å and $L = 340$ Å. The difference between the values for the radius of the cylinder determined by the X-ray and neutron scattering methods is attributed to differences in contrast variation effects between

TABLE 7: In Situ SAXS and ex Situ SANS Study of the Crystallization of Silicalite at 100 °C[a]

				form factor parameters		
time/h	R_g/Å	R_c/Å	$R = \sqrt{2}R_c$	R	L	R_g (calc)
			In Situ SAXS			
0−2	51	29	41	36	141	48
2−4	69	30	42	39	199	64
4−6	76	32	45	40	252	78
6−8	83	32	45	41	310	94
8−10	81	32	45	42	329	99
10−12	93	33	47	43	330	100
12−14	90	32	45	43	325	99
14−16	92	32	45	44	325	99
16−18	94	32	45	44	325	99
18−20	94	32	45	43	331	100
			Ex Situ SANS			
3	57	14	19	21	166	49
5	66	13	18	22	238	71
8	71	15	21	22	240	71
11	78	17	24	22	256	76
14	87	21	30	29	310	92
19	93	22	31	30	302	90
22	88	25	35	34	364	107
26	91	24	34	34	356	105

[a] Note $R_g^2 = R^2/2 + L^2/12$.

the two different types of radiation and will be discussed at greater length below.

The distance distribution function, *P(r)*, also provides evidence supporting the formation of cylindrical particles during the nucleation period. Figure 11 shows the *P(r)* taken at different heating times. Clearly, the *P(r)* is characteristic of a cylindrical particle where the length of the cylinder is indicated by the largest r for which $P(r) = 0$, and the diameter of the cross section is approximated by the inflection point following the maximum. From the plots it can be seen that the diameter of the cylinders formed during this period increases from approximately 67 to 84 Å, and the length of the cylinder increases from 156 to 304 Å, thereby supporting the results obtained from the cylindrical form fitting study.

Scanning Electron Microscopy. Scanning electron micrographs of freeze-dried samples taken from solutions heated for 8 and 19 h are shown in Figure 12a,b, respectively. For the sample heated for 8 h, elliptical shaped particles approximately 200 Å in diameter and 400 Å in length are observed embedded in the TPA/bromide/silicate matrix. The apparent size of these particles is larger than the average size (310 Å long and 82 Å in diameter) deduced from the scattering measurements on the corresponding solution (SAXS results of Table 7). We attribute this discrepancy to the aggregation of particles *during* the freeze-drying process, with the aggregates of two or three particles being the most prominent in the micrograph image. Figure 12b clearly displays the morphology of the 5000 Å particles that are formed with further heating. The micrograph shows how the aggregation of much smaller particles gives rise to the larger silicalite crystals which display an aspect ratio of 1.5. Figure 12c, which was also taken from the sample heated for 19 h, provides another example of the aggregate structure of the silicalite crystals.

Proposed Model for the Crystallization Process. A particularly striking aspect of the above analyses and results is the cylindrical growth behavior of the TPA−silicalite nuclei. As seen in Table 7, the average radius of the cylindrical particles is essentially invariant after the initial 2 h of heating at 100 °C, while the average length of the cylinders increases steadily. This suggests that the nuclei might be growing by the sequential, coaxial fusion of cylindrical primary nuclei whose sizes were

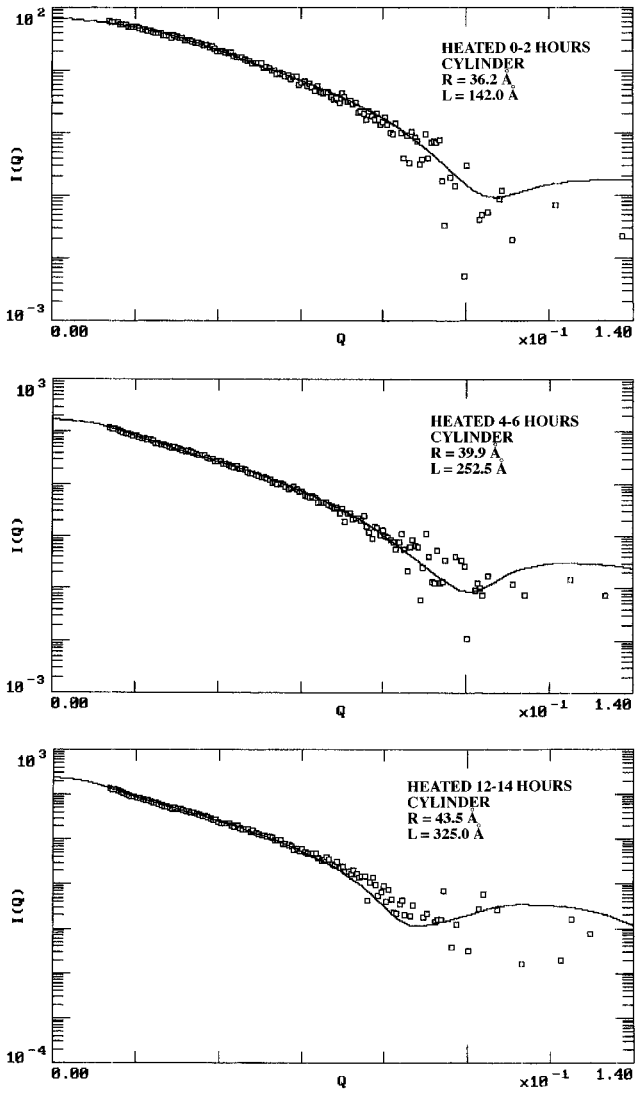

Figure 9. Cylindrical form factors fitted to SAXS data collected during different stages of the synthesis of silicalite: (A, top) 0−2 h heating, (B, middle) 4−6 h, and (C, bottom) 12−14 h of heating.

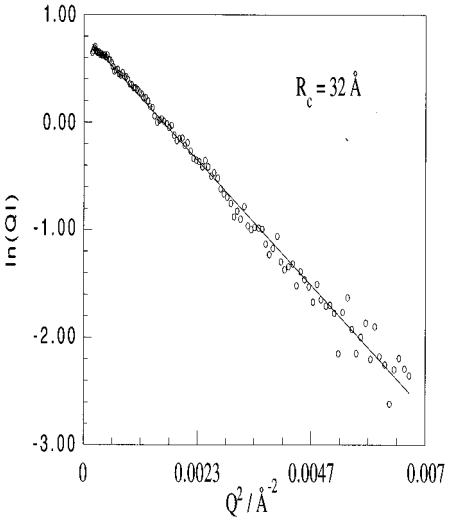

Figure 10. "Guinier plot" for a cylindrical-shaped particle from SAXS data taken during the 12−14 h heating period.

established in the early stages of the nucleation process. We have preliminary evidence from small-angle X-ray scattering from solutions aged at room temperature that these primary nuclei could develop in the synthesis solution before heating.

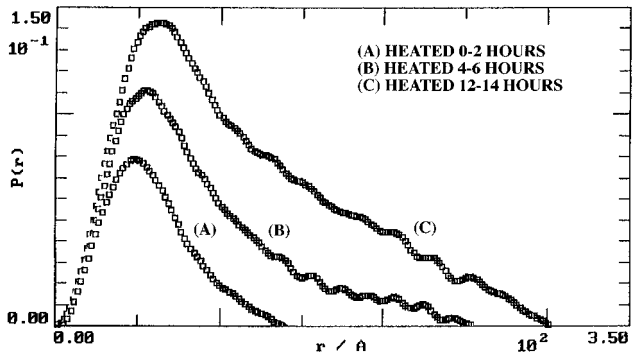

Figure 11. Distance distribution functions calculated from SAXS data at different heating times.

We are seeking to define this primordial stage of the crystallization from the scattering properties of aged, unheated synthesis solutions and from in situ nuclear magnetic resonance (NMR) spectroscopy. These experiments are in progress and the results will be reported elsewhere. The preliminary evidence supports the notion of an early phase of the process, (after heating has begun) during which the primary nuclei are established.

The major stages of the process are therefore proposed to be as follows: (1) a short initial period of formation of cylindrical primary nuclei, with $R_g < 43$ Å, that incorporate TPA and silicate in a structure that has the MFI framework geometry; (2) an induction period during which primary nuclei fuse coaxially and the resulting fused nuclei, now designated primary crystallites, grow to an average length of 330 Å while maintaining an average diameter of 83 Å; (3) a rapid crystal growth period during which primary crystallites fuse, maintaining a strong degree of long-range orientational order, to form ellipsoidal crystals that attain ultimately near-micron size. These crystals give silicalite powder X-ray diffraction patterns. If the aggregation were disordered one would expect greater line broadening in the XRD pattern. Evidence supporting the ordered aggregation was also found in the SEM micrographs (Figure 12b,c). The twinning of the crystal masses seen in the SEM micrographs mirrors the intergrowths commonly seen on the (010) face of large crystals, thereby suggesting that a dominant orientation (with a mosaic spread) prevails in the secondary aggregation.

There are a number of additional details that we deduce from the analyses. We attach some significance to the discrepancy observed between the radii of the cylindrical particles during the induction period as determined by the two scattering techniques (Table 7). We propose that the smaller radii obtained from the SANS measurements and analyses are due to an internal structure of the cylindrical particles consisting of a core with an annular shell, where the radii of the cores are given by the SANS results, while the SAXS results yield the combined radii of the cores with their shells. In this model, the cores are compact and have the complete, well-organized silicalite framework structure with encapsulated TPA cations. The annular shells, however, are highly defected and have a substantial fluid content with the D_2O/H_2O composition of the solvent. The cores would therefore exhibit a scattering contrast with respect to the shells (and the fluid medium). Jansen et al.[24] have found that crystal growth in the MFI structure is fastest along the *c* axis direction because the framework layers with high tetrahedral density are the *ac* and *bc* planes and crystal growth is slower in directions perpendicular to these planes. Similar trends in the growth of silicalite crystals have been reported by Iwasaki *et al.*[13,25] We surmise that the cylindrical axes of these primary nuclei lie along the *c* axis of the MFI

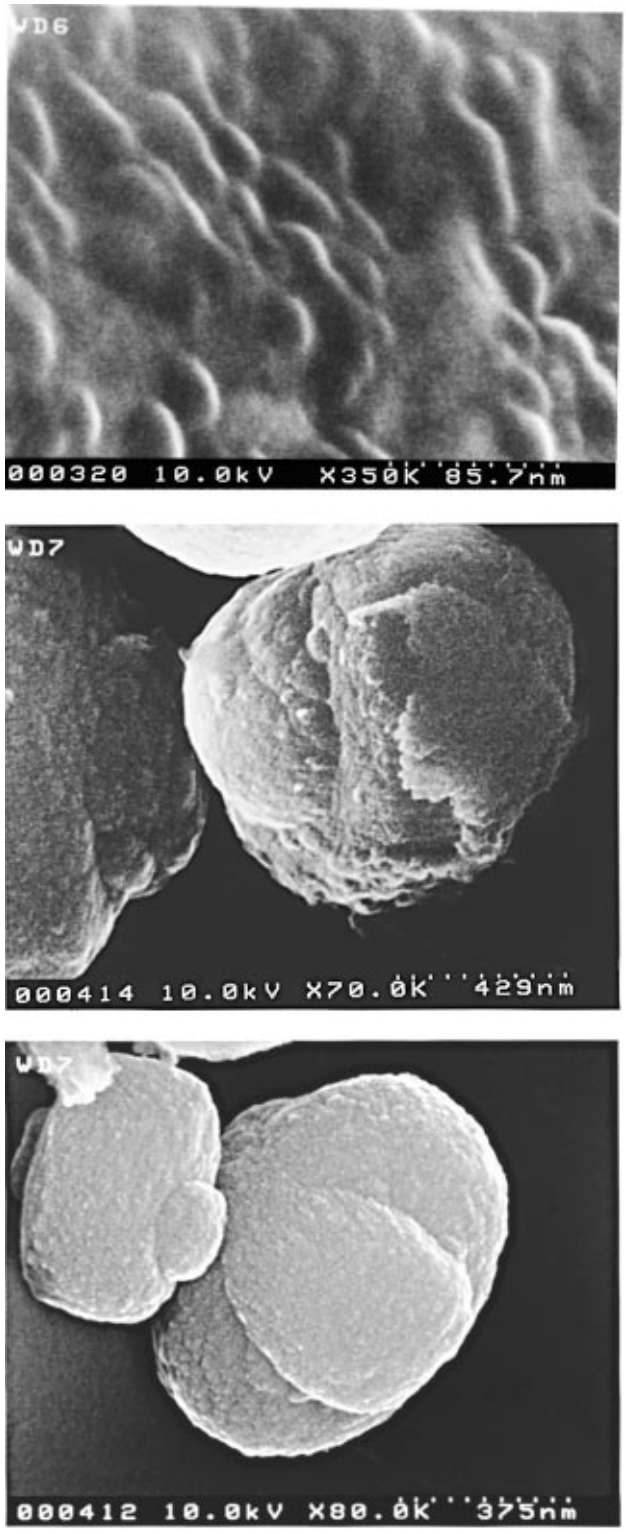

Figure 12. Scanning electron micrographs of freeze-dried samples taken from the synthesis mixture after (A, top) 8, (B, middle) 19, and (C, bottom).

structure, so that the primary crystallites grow by end-to-end fusion of the primary nuclei such that the growth is in the *c* axis direction. The ends of the cylinders are in the *ab* plane of the crystallite, and the radial dimensions of the cores (for nucleation at 100 °C) would then correspond to a domain of 2 × 2 unit cells along the *a* and *b* axes. The size of the cores in the primary nuclei might be dependent on the crystallization temperature, but we have not attempted to determine this.

We suggest that the end of the induction period (after ≈12 h at 100 °C) corresponds to the termination of the growth of the

primary crystallites and indicates that the assembly of all the primary nuclei into primary crystallite particles has been completed. Formation of the primary nuclei does not continue throughout the process so that the number of particles would be constant after the induction period. Twomey *et al.*[10] have previously found that the number density of the particles remained constant after the induction period in light scattering studies of TPA−silicalite crystallization from concentrated hydroxide solutions. In our proposed picture, the end of the induction period prompts the ordering of the disordered annular shell of the cylindrical primary crystallites. This is indicated by the abrupt increase of the diameters of the cylindrical particles in solution between 11 and 14 h of heating, as measured by the SANS experiment (Table 7). At this time, the aggregation of primary crystallites begins, this process having been delayed to this point because of the disordered nature of the curved cylindrical particle surfaces. This is reflected in the rapid increase in the average particle size in solution as measured by the DLS experiment.

There are obvious similarities between our proposed picture and those proposed by Regev et al.[7] and by Dokter et al.[8,9] in previously reported SAXS and SANS studies. In particular, the recurring premise is that of the formation of primary nuclei that aggregate in one or more subsequent stages. However, there are significant difference in the details of the several proposed models that we now note. We first point out that the study of Regev et al. was made on the supernate from a gel crystallization experiment so that the conditions are somewhat different from ours. Their model posits that globular primary nuclei exist in their unheated supernate solution and that these aggregate into cylindrical particles that increase in both length and diameter. The cylindrical aggregates are amorphous until they sediment from the supernate, and the reorganization into the MFI crystalline structure occurs slowly in the precipitated solid phase. Dokter *et al.*[8] studied crystallization from a homogeneous, hydroxide-based synthesis solution, so that their crystallization conditions more closely resemble those employed in our study. We should note, though, that the concentration of their synthesis solution was very high, with the following mole ratios: SiO_2:TPA:H_2O = 4.1:1.0:45. The effective molal concentration of TPA in this synthesis solution is 1.23; at this concentration in a TPA bromide solution there would be a significant concentration of dimerized ion pairs and larger aggregates even in the absence of the silicate component.[21] In the crystallization model proposed by Dokter et al.,[8] primary nuclei aggregate and densify into an amorphous structure. These amorphous structures in turn aggregate again, and the crystallization occurs in the amorphous structures following the secondary aggregation. There follows a subsequent densification stage which results in smooth, crystalline particles. This essentially means that the crystallization is of the gel transformation type, despite the homogeneous character of the synthesis solution.

The major differences between our proposed crystallization model and those[8,9] summarized above are clear. We identify an early stage in which formation of primary nuclei is completed, and we posit that the MFI framework organization is already developed during the period of formation of the primary nuclei, so that the primary crystallites present at the end of the induction period have a core structure which is that of MFI. This is confirmed by the observation of the characteristic framework vibration at 550 cm^{-1} in the IR spectrum. The subsequent ordering of the disordered shells of the primary crystallites accompanies the aggregation of primary crystallites in the crystallization stage. This is responsible for the plateau and decrease in $I(0)$ obtained from SAXS data beyond 12 h of heating. The radii of these particles must be greater than 200 Å as they are not detected by SAXS and SANS. The DLS results support this model in that, during the time period when $I(0)$ is reaching a maximum, a corresponding increase in the crystal growth rate is observed. This also corresponds to the period when turbidity begins to appear in the synthesis solution. From Figures 4 and 5 the onset of crystallization of silicalite at 100 °C occurs approximately after 12 h of heating.

Conclusions

Using small-angle X-ray and neutron scattering, we have been able to directly monitor the transformations occurring during the induction period for the crystallization from a homogeneous synthesis solution of silicalite templated by TPA cations. In situ SAXS measurements, when complemented by SANS measurements, have afforded novel insights into the detailed progression from nucleation to sedimentation of crystalline aggregates. We have accurately measured over a range of temperatures the rate of growth of crystal nuclei formed in the clear homogeneous preparation, with no apparent involvement of a gelatinous intermediate phase; this has yielded thermodynamic and kinetic parameters. Our SANS contrast variation study has provided direct evidence of the incorporation of the template in the nuclei, while complementary infrared spectroscopy measurements have confirmed that the particles present in colloidal solution at the end of the induction period have the silicalite framework structure. The DLS study has complemented our SAXS study in monitoring the growth of silicalite crystals during the latter stage where aggregation of primary crystallites occurs and has helped our understanding of the processes involved in the nucleation and crystallization of silicalite.

Acknowledgment. This work has benefited from the use of the Intense Pulsed Neutron Source at Argonne National Laboratory (ANL) which is funded by the U.S. Department of Energy, BES-Materials Science, under Contract W-31-109-ENG-38. We thank Dr. P. Thiyagarajan and Mr. D. Wozniak for assistance with the experiments at IPNS and Jill Lombaer for her assistance with this project at ANL. We also thank Dr. S. King and Dr. A. S. Brown for assistance with the LOQ measurements at the Rutherford Appleton Laboratory, UK. We thank the Electron Microscopy Unit at the Australian National University as well. Work at ANL is supported by the U.S. Department of Energy, Office of Basic Energy Sciences−Materials Science. A travel grant through ISTAC/ANSTO Access to Major Facilities Program for J.N.W. is gratefully acknowledged.

References and Notes

(1) Lok, B. M.; Cannan, T. R.; Messina, C. A. *Zeolites* **1983**, *3*, 282.
(2) Iton, L. E.; Trouw, F.; Brun, T. O.; Epperson, J. E.; White, J. W.; Henderson, S. J. *Langmuir* **1992**, *8*, 1045.
(3) Dougherty, J.; Iton, L. E.; White, J. W. *Zeolites* **1995**, *15*, 640.
(4) Watson, J. N.; Iton, L. E.; White, J. W. *Chem. Commun.* **1996**, 2767.
(5) Gabelica, Z.; Nagy, J. B.; Debras, G.; Derouane, E. G. In *Proceedings of the Sixth International Zeolite Conference*; Olson, D., Bisio, A., Eds.; Butterworths: Guilford, 1984.
(6) Davis, M. E.; Lobo, R. F. *Chem. Mater.* **1992**, *4*, 756.
(7) Regev, O.; Cohen, Y.; Kehat, E.; Talmon, Y. *Zeolites* **1994**, *14*, 314.
(8) Dokter, W. H.; van Garderen, H. F.; Beelen, T. P. M.; van Santen, R. A.; Bras, W. *Angew. Chem., Int. Ed. Engl.* **1995**, *34*, 73.
(9) Dokter, W. H.; Beelen, T. P. M.; van Garderen, H. F.; Rummens, C. P. J.; van Santen, R. A.; Ramsay, J. D. F. *Colloids Surf., A* **1994**, *85*, 89.
(10) Twomey, T. A. M.; Mackay, M.; Kuipers, H. P. C. E.; Thompson, R. W. *Zeolites* **1994**, *14*, 162.
(11) Schoeman, B. J.; Sterte, J.; Otterstedt, J.-E. *Zeolites* **1994**, *14*, 568.

(12) Persson, A. E.; Schoeman, B. J.; Sterte, J. and Otterstedt, J.-E. *Zeolites* **1994**, *14*, 557.
(13) Iwasaki, A.; Hirata, M.; Kudo, I.; Sano, T.; Sugawara, S.; Ito, M. and Watanabe, M. *Zeolites* **1995**, *15*, 308.
(14) Schoeman, B. J. *Zeolites* **1997**, *18*, 97.
(15) Flanigen, E. M.; Bennett, J. M.; Grose, R. W.; Cohen, J. P.; Patton, R. L.; Kirchner, R. M.; Smith, J. V. *Nature* **1978**, *271*, 512.
(16) von Ballmoos, R. *The 18O-Exchange Method in Zeolite Chemistry, Synthesis, Characterisation and Dealumination of High Silica Zeolites*; Otto Salle Verlag GmbH & Co., Frankfurt am Main, 1981; p 83.
(17) Wirth, H. E. *J. Phys. Chem.* **1967**, *71*, 2922.
(18) Aldissi, M.; Henderson, S.; White, J. W.; Zemb, T. *Mater. Sci. Forum* **1988**, *27/28*, 437.
(19) Jacrot, B. *Rep. Prog. Phys*. **1976**, *39*, 911.
(20) Suparno, Deurloo, K.; Stamatelopolous, P.; Srivastva, R.; Thomas, J. C. *Appl. Opt.* **1994**, *33*, 7200.
(21) Barrer, R. M. *Hydrothermal Chemistry of Zeolites*; Academic Press: New York, **1982**; p 154.
(22) Burkett, S. L.; Davis, M. E. *Chem. Mater*. **1995**, *7*, 920.
(23) Jacobs, P. A.; Derouane, E. G.;d and Weitkamp, J. *Chem. Comm*. **1981**, 591.
(24) Jansen, J. C.; Engelen, C. W. R.; van Bekkum, H. In *Zeolite Synthesis*; Occelli, M. L., Robson, H. E., Eds.; ACS Symp. Ser. 398; American Chemical Society: Washington, DC, 1989; p 257.
(25) Iwasaki, A.; Hirata, M.; Kudo, I.; Sano, T. *Zeolites* **1996**, *16*, 35.